

## Effect of noise in the direction of motion over the spatial distribution and proliferation of migrating cell collectives

Jonathan E. Dawson<sup>1,2</sup> and Abdul N. Malmi-Kakkada<sup>1,\*</sup><sup>1</sup>*Department of Physics and Biophysics, Augusta University, Augusta, Georgia 30912, USA*<sup>2</sup>*Department of Engineering and Physics, Whitworth University, Spokane, Washington 99251, USA*

(Received 25 July 2023; revised 24 April 2024; accepted 31 May 2024; published 11 July 2024)

A variety of living and nonliving systems exhibit collective motion. From swarm robotics to bacterial swarms, and tissue wound healing to human crowds, examples of collective motion are highly diverse but all of them share the common necessary ingredient of moving and interacting agents. While collective motion has been extensively studied in nonproliferating systems, how the proliferation of constituent agents affects their collective behavior is not well understood. Here, we focus on growing active agents as a model for cells and study how the interplay between noise in their direction of movement and proliferation determines the overall spatial pattern of collective motion. In this agent-based model, motile cells possess the ability to adhere to each other through cell-cell adhesion, grow in size, and divide. Cell-cell interactions influence not only the direction of cell movement but also cell growth through a force-dependent mechanical feedback process. We show that noise in the direction of a cell's motion has striking effects on both the emergent spatial distribution of cell collectives and proliferation. While higher noise strength leads to a random spatial distribution of cells, we also observe increased cell proliferation. On the other hand, low noise strength leads to a ringlike spatial distribution of cell collectives together with lower proliferation. Our findings provide insight into how noisy cell motion determines the local spatial organization of cells with consequent mechanical feedback on cell division impacting cell proliferation due to the formation of cell clusters.

DOI: [10.1103/PhysRevResearch.6.033054](https://doi.org/10.1103/PhysRevResearch.6.033054)

### I. INTRODUCTION

The importance of the coordination between cell division and cell migration is recognized in multiple physiological processes, such as tissue regeneration and inflammation, as well as in pathological conditions, such as cancer metastasis [1,2]. Because cell migratory and proliferation patterns determine how cells organize spatially over time, understanding the underlying biophysical mechanisms is crucial for our ability to direct spatial organization of cells in a customizable manner. This has important implications for understanding tissue regeneration and cancer invasion [2,3].

With the emergence of multiplexed tissue imaging modalities that allow for quantification of cell proliferation at single-cell resolution [4,5], it is now possible to determine how cell-cell interactions influence cell proliferation [6] from spatial map of single cells, together with higher-order relationships in space. In a cell collective, spatial constraints due to crowding limits the space available to a cell due to the presence of neighboring cells and thus imposes constraints on cell proliferation [7–9]. Similarly, collective cell migration, a foundational collective behavior in living systems, involves both the interaction of a cell with its environment as well as its

neighbors [3,10–13]. For instance, cell-cell adhesion impacts cell dynamics and the spatial coordination of cells in a tissue [3,14]. Despite the importance of cell-cell interactions, the relation between cell migration driven spatial organization and how it impacts cell proliferation due to physical constraints remains unclear. Given that cells are active particles that transduce stored energy into mechanical motion, an interesting question that arises is how the coordination between cell migration and proliferation influences the spatial organization of cell collectives. While cell growth, cell division, and cell migration are highly complex processes, involving a large network of intracellular signaling pathways [15], here we focus on the biophysical intercellular interactions that are known to play a key role in cell collective migration and proliferation [16–20].

Mathematical and computational models of cell behaviors have contributed to a quantitative understanding of collective cell migratory behaviors and their underlying mechanisms [13,21–26]. Pioneering work by Vicsek and co-workers showed that the collective dynamics of self-driven or active particles emerge from a form of interparticle coupling: a simple rule that an individual constituent's direction of motion is aligned with the average direction of motion of its neighbors [27]. Both the number density of agents and noise in the direction of their movement are key parameters that regulate spatial patterns of collective motion. Distinct from earlier studies, we focus on studying the coupling between noise in the directionality of cell migration and cell division. The effect of cell division and cell death on collective cell movement has been studied in mean-field dynamical theoretical models [28,29]

\*Contact author: [amalmikakkada@augusta.edu](mailto:amalmikakkada@augusta.edu)

with experiments showing that cell growth and division can influence cell migratory behavior [30]. Our recent work in the context of freely expanding three-dimensional (3D) cell collectives [17,18] showed that the intercellular forces give rise to heterogeneous cell motility patterns between the boundary and the interior of the cell collective. In addition to cell-cell mechanical interactions, we anticipate that the noise in the cell movement direction may generate complex spatial distribution patterns with novel implications for how cells divide.

To elucidate the role of noise in self-organization and proliferation in a migrating cell collective, we study a system of self-propelled particles with the capacity to proliferate, and whose motion is governed by local alignment rules. Each cell can grow in size and divide upon reaching a critical size. Cells in direct contact through cell-cell adhesion exert a force, which when it exceeds a threshold inhibits cell growth and prevents cell division. Such mechanical feedback on cell proliferation is in agreement with recently reported experimental observations [31–33]. Cell division events in this model scramble the velocity orientation of dividing cells. By combining mechanical and alignment cell-cell interactions with cell division events, our model is highly relevant to biological systems, such as cells, which possess an inherent capability to proliferate and migrate. Our work provides insight into the fundamental features of expanding active matter. Notably, we discover that noise in the direction of a cell's motion not only influences the spatial structure of cell collectives but also determines the ability of cells to proliferate.

## II. MODEL DESCRIPTION AND SIMULATION DETAILS

Here we introduce the computational model we implemented to study the growth and migration of cell collectives in two dimensions (2D). The off-lattice agent-based model and the simulation scheme are adapted from our previous work on three-dimensional tumor growth [9,17–19,34]. Such off-lattice simulations are widely used to recapitulate experimentally observed features of individual cell dynamics within cell collectives [35,36]. Individual cells are modeled as soft disklike motile particles of radius  $R$ , Fig. 1(a), which grow stochastically in time  $t$ , and upon reaching a critical size, undergo division into two daughter cells. In addition to its radius,  $R_i(t)$ , the state of each cell  $i$  is characterized by its position  $\mathbf{r}_i(t)$  and direction of motion  $\theta_i(t)$ , Fig. 1(a) (inset). The dynamics of the proliferating and migrating cell collective are governed by the following three factors: (a) mechanical forces arising from two-body interactions, (b) active processes due to cell growth, division, and death, and (c) active self-propulsion with directional noise together with neighbor interactions that align the direction of cell motion with its neighbors. The model implementation of these factors is explained in detail below.

### A. Mechanical cell-cell interactions

Individual cells interact with short-ranged forces, consisting of two terms: elastic force (repulsion) and adhesion (attraction). The elastic force,  $F_{ij}^{\text{el}}$ , between any pair of cells  $i$

and  $j$  of radii  $R_i$  and  $R_j$  discourages spatial overlap between cells [Fig. 1(b)] and is given by [17,36]

$$F_{ij}^{\text{el}} = \frac{h_{ij}^{3/2}}{\frac{3}{4} \left( \frac{1-\nu_i^2}{E_i} + \frac{1-\nu_j^2}{E_j} \right) \sqrt{\frac{1}{R_i(t)} + \frac{1}{R_j(t)}}}, \quad (1)$$

where  $\nu_i$  and  $E_i$  are the Poisson ratio and elastic modulus of the  $i$ th cell.  $h_{ij}$  defined as  $\max[0, R_i + R_j - |\vec{r}_i - \vec{r}_j|]$  is the virtual overlap distance between the two cells [17]. Biological cells adhere to their immediate physical neighbors through cell adhesion molecules, Fig. 1(c). The adhesive force,  $F_{ij}^{\text{ad}}$ , between a pair of interacting cells depends on the contact length between two cells,  $l_{ij}$  (see Supplemental Material [37], SI-I, for the analytical calculation of  $l_{ij}$ ), and is given by [9,17,36],

$$F_{ij}^{\text{ad}} = f^{\text{ad}} l_{ij} \frac{1}{2} (c_i^{\text{rec}} c_j^{\text{lig}} + c_j^{\text{rec}} c_i^{\text{lig}}), \quad (2)$$

where  $c_i^{\text{rec}}$  ( $c_i^{\text{lig}}$ ) is the receptor (ligand) concentration (assumed to be normalized with respect to the maximum receptor or ligand concentration so that  $0 \leq c_i^{\text{rec}}, c_i^{\text{lig}} \leq 1$ ). The coupling constant  $f^{\text{ad}}$  allows us to rescale the adhesion force to account for the variabilities in the maximum receptor and ligand concentrations.

Both the elastic and the adhesive forces act along the unit vector  $\mathbf{n}_{ij}$ , pointing from the center of cell  $j$  to the center of cell  $i$ . The net force ( $\mathbf{F}_i$ ) on the  $i$ th cell is the vectorial sum of the elastic and adhesive forces that the neighboring cells exert on it,

$$\mathbf{F}_i = \sum_{j \in NN(i)} \mathbf{f}_{ij} = \sum_{j \in NN(i)} (F_{ij}^{\text{el}} - F_{ij}^{\text{ad}}) \mathbf{n}_{ij}. \quad (3)$$

Here,  $j$  is summed over the number of nearest neighbors  $NN(i)$  of cell  $i$ . The nearest neighbors of cell  $i$  are all the cells that satisfy the criterion  $h_{ij} > 0$ . The net force due to finite area exclusion (elastic term) and cell-cell adhesion is dampened by an effective friction contribution which comes from (i) the interaction of a cell with the extracellular matrix (ECM), and (ii) cell-cell adhesion. The cell friction coefficient is given by

$$\gamma_i(t) = \gamma_i^{\text{ECM}}(t) + \gamma_i^{\text{ad}}(t). \quad (4)$$

The cell-ECM friction coefficient is assumed to be given by the modified Stokes relation,

$$\gamma_i^{\text{ECM}}(t) = 6\pi \mu R_i(t), \quad (5)$$

where  $\mu$  is the viscosity due to the ECM. We consider additional damping of cell movement due to adhesive forces given by

$$\gamma_i^{\text{ad}} = \zeta^{\text{max}} \sum_{j \in NN(i)} \left[ \frac{l_{ij}}{2} \left( 1 + \frac{\mathbf{F}_i \cdot \mathbf{n}_{ij}}{|\mathbf{F}_i|} \right) \frac{1}{2} (c_i^{\text{rec}} c_j^{\text{lig}} + c_j^{\text{rec}} c_i^{\text{lig}}) \right], \quad (6)$$

where,  $\zeta^{\text{max}}$  is the adhesive friction coefficient and  $\mathbf{F}_i$  is as defined in Eq. (3). Note that the added friction coefficient

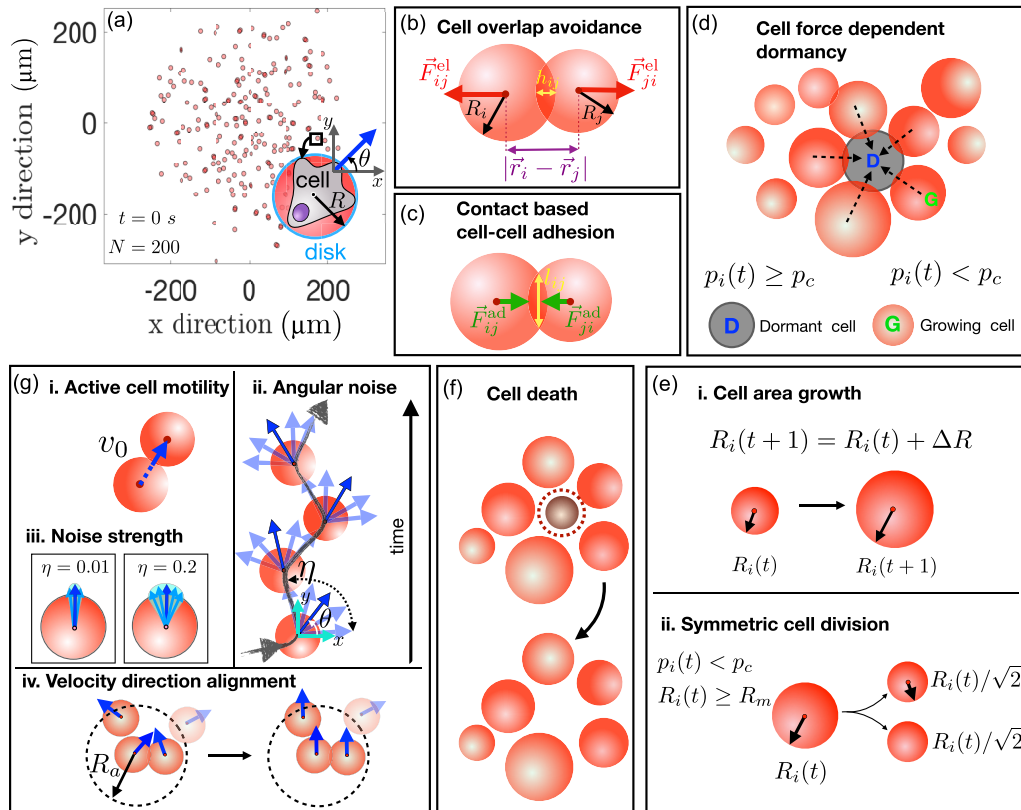


FIG. 1. Self-propelled particle model for a two-dimensional (2D) proliferating cell collective. Cells are represented as motile 2D circular disks that move with an active speed of  $v_0$ . Individual cells can grow in size and divide over time. (a) Initial snapshot of the simulation is shown where each dot represents a cell (see inset). Cell motility leads to the spatial spread of the collective, which is quantified by tracking individual cell positions. (b) When two cells overlap, each experience an elastic force  $\mathbf{F}_{ij}^{el}$ , where  $i$  and  $j$  are the cell indices. The magnitude of the elastic force is proportional to the degree of overlap  $h_{ij}$ . (c) Cell adhesion in the model is mediated by receptors on the cell membrane. In this simplistic model, where the receptors and ligands are assumed to be evenly distributed on the cell surface, the magnitude of the adhesive force is assumed to scale as a function of their contact length  $l_{ij}$ . (d) If the force per unit length  $p_i$  that the  $i$ th cell experiences (due to neighbor cell contacts) exceeds a critical threshold  $p_c$ , i.e.,  $p_i(t) \geq p_c$ , then that cell enters the dormant state (D). (e) (i)–(ii) If  $p_i(t) < p_c$ , the cells grow (G) until they reach the mitotic radius  $R_m$ . At that stage, the cell undergoes area-conserved symmetric cell division, giving rise to two new cells with the same radii. A cell that is dormant at a given time can transit from that state at subsequent times. (f) The cells can undergo apoptosis at a rate  $k_d$ . Upon apoptosis, the cell is removed from the cell collective. (g) Together with proliferation, the cells are endowed with the capability to self-propel. (i) Motility of each cell in the collective is characterized by a constant active speed  $v_0$  along the direction, or orientation, of motion  $\theta$ . (ii)–(iv) The net direction of cell movement depends on the angular noise (light blue arrows). The strength of the angular noise  $\eta$  determines how much a cell deviates from its current direction of motion in the next instant (iii). (iv) Additionally, the direction of motion of a cell depends on all of its nearest neighbors over a spatial range of length  $R_a$  together with the net intercellular interaction force (due to repulsion and adhesion).

$\gamma_i^{ad}$  is proportional to the cell-cell contact length  $l_{ij}$ , implying that the damping of cell movement due to this friction term is proportional to the number of cells that cell  $i$  is in contact with at any given time.

## B. Cell proliferation

In our model, the cell number grows due to the imbalance between cell division and apoptosis. At any point in time cells are either in the growth (G) phase in which the cell area increases over time, or in the dormant (D) phase whereby the cell area growth is arrested, Fig. 1(d). Whether a cell continues in the growth phase or enters the dormant phase is determined by the total force per unit length acting on a cell due to the neighboring cells. The total external force per unit length,  $p_i$ ,

that a cell experiences is calculated using

$$p_i(t) = \sum_{j \in NN(i)} \frac{|\mathbf{f}_{ij} \cdot \mathbf{n}_{ij}|}{l_{ij}}. \quad (7)$$

If  $p_i(t)$  on a cell  $i$  at any given time  $t$  is smaller than a threshold value,  $p_c$ , the cell grows in size, Fig. 1(e)(i). However, if  $p_i(t) > p_c$ , the cell enters dormancy, Fig. 1(d). Hence, depending on the ratio of  $\frac{p_i(t)}{p_c}$ , cells can switch between the two states of dormancy and area growth. A cell grows in size by increasing its radius in a stochastic manner sampled from a Gaussian distribution with the mean rate  $\frac{dR_i}{dt} = (2\pi R_i)^{-1} g_a$ , where  $g_a$  is the cell area growth rate given by

$$g_a = \frac{\pi R_m^2}{2\tau}. \quad (8)$$

Here,  $\tau$  is the benchmark cell cycle time and  $R_m$  is the mitotic radius at which a cell divides (see Table I).  $g_a = 0.039 \mu\text{m}^2/\text{s}$  for  $\tau = 1000 \text{ s}$  and the mean value  $\frac{dR_i}{dt}$  is in the range 0.0012–0.0017 (depending on cell size) with a standard deviation of  $10^{-7}$ . Therefore, at each time step, the growth rate depends on both the size of the cell as well as the standard deviation of the Gaussian distribution (which is small compared to the mean). We assume that a cell divides into two daughter cells upon reaching  $R_m = 5 \mu\text{m}$ , giving rise to two identical daughter cells, each with radii  $R_d = \frac{R_m}{\sqrt{2}}$ , ensuring area conservation, Fig. 1(e)(ii). Immediately following a division event, the daughter cells are displaced by a distance  $d_{\text{max}} = (\frac{\sqrt{2}-1}{\sqrt{2}}) \times 5 \mu\text{m} = 1.46 \mu\text{m}$ , and the whole growth process is repeated. Hence, a key timescale in the simulation is  $\tau$ , set to be  $\sim 0.27$  hours. Force feedback on proliferation leads to effectively longer cell division times in the range of 1–2 hours as we discuss later. Cell division times can vary depending on the cell type. As immune cells such as  $\text{CD8}^+$  T cells divide over a timescale as short as 2 hours [38], we are within the plausible range of cell division times. As daughter cells are assigned completely random active velocity orientations, cell division events tend to scramble the orientational order of the cells. Death of a cell takes place in the simulation leading to a randomly selected cell being removed from the collective, Fig. 1(f). The death rate is set to  $k_d = 10^{-20} \text{ s}^{-1}$  and occurs in a probabilistic manner. If the number drawn from a random uniform distribution is less than  $k_d dt$ , this leads to cell death. Owing to  $k_d \ll \frac{1}{\tau}$ , we are simulating a rapidly growing system of cells.

### C. Neighbor velocity alignment and fluctuation in the direction of motion

The cell position,  $\mathbf{r}_i(t)$ , is described through the coordinates  $(x_i(t), y_i(t))$ . Cell self-propulsion velocity is  $\mathbf{v}_i(t) = v_0 \mathbf{s}_i(t)$ , where  $v_0$  is the cell migration speed, and  $\mathbf{s}_i(t) = (\cos \theta_i(t), \sin \theta_i(t))$  is the unit vector representing the direction of cell migration.  $\theta$  is the angle that the cell makes with the horizontal axis in the laboratory frame. Each cell in this model is endowed with active motility that propels the cell in a given direction with a fixed speed  $v_0$ , Fig. 1(g)(i).

The directional alignment, and thus the overall direction of a cell's motion, is hampered by an angular white noise uniformly distributed in range  $\xi_i \in [-\frac{\pi}{2}, +\frac{\pi}{2}]$  with  $\langle \xi_i^t \rangle = 0$  and  $\langle \xi_i^t \xi_j^{t'} \rangle \sim \delta_{ij} \delta_{tt'}$  and whose strength is given by  $\eta$ , Fig. 1(g)(ii). As the effective noise is given by  $\eta \xi_i$ ,  $\eta = 0.2$  implies random fluctuations occur in the range  $[-\frac{\pi}{10}, +\frac{\pi}{10}]$ , Fig. 1(g)(iii), whereas,  $\eta = 0.01$  results in random fluctuations in the range  $[-\frac{\pi}{200}, +\frac{\pi}{200}]$ , Fig. 1(g)(iii). The noise term represents fluctuations in the direction of a cell's motion. In biological systems, such as cells, there are many sources of such noise in the direction or orientation of cell movement. Stochasticity intrinsic to cellular movement, such as due to limitations in cellular sensing or active shape remodeling during cell migration [39,40], is an example.

In addition to the forces due to nearest-neighbor mechanical interactions, as described in (a), each cell interacts with its neighbors in a manner that aligns its velocity with its neighbors, Fig. 1(g)(iv). The neighbors which contribute to

the velocity realignment of cell  $i$  are all those cells in the collective within a distance satisfying  $|\mathbf{r}_i(t) - \mathbf{r}_j(t)| < R_a$ , where  $|\dots|$  is the vector magnitude. We set  $R_a = 10 \mu\text{m}$  which limits velocity realignment to occur with neighbors that are located close to a given cell. We then obtain the average orientation of the velocities of all the cells that satisfy the nearest-neighbor criteria and assign that to the velocity orientation of cell  $i$ . The cell velocity realignment with its neighbors influences its direction of motility, such that cells in a cluster tend to move in the same direction, Fig. 1(g)(iv). Such contact-based modulation of cell velocity is known to play a role in the collective migration of electrically stimulated cells [20].

The complex dynamics of each cell in the collective involves active motility, area growth, division, and death. In the low Reynolds number limit, the equation of motion is fully described by the following rules:

$$r_i^x(t + \Delta t) = r_i^x(t) + v_i^x(t)\Delta t + \frac{F_i^x(t)}{\gamma_i(t)} \Delta t, \quad (9)$$

$$r_i^y(t + \Delta t) = r_i^y(t) + v_i^y(t)\Delta t + \frac{F_i^y(t)}{\gamma_i(t)} \Delta t, \quad (10)$$

$$\theta_i(t + \Delta t) = \arg \left[ \sum_{j \in |\mathbf{r}_i(t) - \mathbf{r}_j(t)| < R_a} \mathbf{v}_j(t) + \mathbf{F}_i(t)/\gamma \right] + \eta \sqrt{\Delta t} \xi_i(t). \quad (11)$$

Equations (9) and (10) describe the evolution of the  $x$  and  $y$  coordinates of a cell  $i$ , governed by an active component that propels the cell with a speed  $v_0$  in the direction  $\theta_i(t)$  and the net force  $\mathbf{F}_i$  on the cell due to its contacting neighbors. We assume that the cell exerts a self-propulsion force which propels it with a constant effective active speed  $v_0$ . We operate in the domain where  $v_0 \gg F_i/\gamma$ , implying that the active velocity dominates the contribution to velocity arising from cell-cell interaction forces; see the Supplemental Material [37], SI-II. Equation (11) describes the orientation dynamics of a cell  $i$ , where  $\theta_i(t + \Delta t)$  is the direction in which the cell moves in the next time step. The net contribution to the direction of a cell's motility comes from (i) orientation realignment, the first term on the right-hand side of Eq. (11), (ii) the interaction forces [discussed in (a)], the second term on the right-hand side of Eq. (11), and (iii) the noise term.  $\arg[\mathbf{c}]$  in Eq. (11) refers to the angle associated with the vector  $\mathbf{c}$ , in polar coordinates, and the sum is taken over all the cells  $j$  within a distance of  $R_a$  of cell  $i$  (including cell  $i$  itself). The net direction in which cell  $i$  moves is given by the angle associated with the net vector, which is obtained by vector addition of  $\mathbf{v}_j$  and the net force  $\mathbf{F}_i$  on the  $i$ th cell. The overall direction is affected by an angular white noise. Due to particular properties of white noise, and finite time-step size in our simulations, discretization of the white noise term includes  $\sqrt{\Delta t}$  [41]. We confirmed that the stochastic cell angular dynamics are independent of the time step  $\Delta t$  (see Supplemental Material [37], SI-III). Next, we checked whether the total number of cells as a function of time depends on  $\Delta t$  (see Supplemental Material, Fig. S4, SI-IV). For  $\eta = 0.01$ , total cell number dynamics shows minimal change with  $\Delta t$  while there is a difference at  $\eta = 0.1$  at later times. We anticipate

TABLE I. The parameters used in the simulation aim to represent biological cells. The cell stiffness value ( $E_i$ ) we consider is in the range of experimentally measured cell stiffnesses [42]. Similarly, the cell active speed is in the correct range for cell migration speed [43,44] and the environmental viscosity parameter we consider ( $\mu$ ) is comparable with micropipette-based tissue viscosity measurements [45,46]. The validity of the cell-cell adhesion strength and  $p_c$  values are discussed in detail in our earlier work [9].

Parameter	Value
Time step ( $\Delta t$ )	5 s
Active cell speed ( $v$ )	0.1 $\mu\text{m/s}$
Critical radius for division ( $R_m$ )	5 $\mu\text{m}$
Environment viscosity ( $\mu$ )	0.005 kg/( $\mu\text{m s}$ )
Adhesive friction coefficient ( $\zeta^{\text{max}}$ )	$10^{-4}$ kg/( $\mu\text{m s}$ )
Benchmark cell cycle time ( $\tau$ )	1000–2000 s
Adhesive coefficient ( $f^{\text{ad}}$ )	$10^{-4}$ $\mu\text{N}/\mu\text{m}$
Mean cell elastic modulus ( $E_i$ )	$10^{-3}$ MPa
Mean cell Poisson ratio ( $\nu_i$ )	0.5
Death rate ( $k_d$ )	$10^{-20}$ $\text{s}^{-1}$
Mean receptor concentration ( $c^{\text{rec}}$ )	0.9 (normalized)
Mean ligand concentration ( $c^{\text{lig}}$ )	0.9 (normalized)
Threshold force ( $p_c$ )	$10^{-4}$ N/m
Noise strengths ( $\eta$ )	0.01–0.2

this to be due to the numerical discretization scheme for  $\theta(t)$  [see Eq. (11)] differing from a simple Euler discretization (see Supplemental Material, SI-IV, for further details).

#### D. Initial conditions

We initiated the simulations by generating 200 nonoverlapping cells, randomly distributed in a circular region within a 2D spatial domain of size  $250 \mu\text{m} \times 250 \mu\text{m}$ . For all future time steps, we consider an open boundary condition. Each cell is assigned an initial orientation of the active velocity, randomly distributed in the domain  $[0, 2\pi]$ . All the parameters are fixed except the noise strength of velocity orientation switching ( $\eta$ ), which we vary from 0.01 to 0.2. The simulated cell aggregate is evolved to  $\sim 10\tau$ , ensuring that we are sampling the long-time regime as compared to division times. Relevant parameters are shown in Table I. We used a time step of 5 s, which is short compared to the elastic timescale  $\tau_{\text{el}} = \gamma/ER$ , depending on the friction coefficient  $\gamma$ , elastic modulus ( $E$ ), and radius ( $R$ ). The particle coordinates were recorded and used to calculate the dynamical observables relevant to the present study.

### III. NOISE IN THE CELL MOTILITY DIRECTION CONTROLS THE SPATIAL DISTRIBUTION OF THE CELL COLLECTIVE

We first sought to understand how noise in the cell motility direction determines the spatial distribution of a growing cell collective. The cell spatial distribution at  $t = 10\,000$  s shows a strong dependence on the noise strength  $\eta$ , Figs. 2(a) and 2(c). For low noise strengths ( $\eta = 0.01$ ) cells are organized into multiple clusters that are spatially distributed in a roughly circular, ringlike pattern, Fig. 2(a) (see Supplemental Material [37], SI-V, for simulation movies). The cells cluster into small

groups mostly along the edge of the ringlike domain while its interior is mostly devoid of cells, Fig. 2(a). By focusing on a single cluster [blue box in Fig. 2(a)], we observe that the constituent cells display highly coordinated motion, wherein each cell moves in roughly the same direction pointing radially outward, as seen from the blue arrows in Fig. 2(a) (inset) and Fig. 2(b). At higher noise strength of  $\eta = 0.2$  the cell spatial distribution changes from the ringlike structure to a diffuse morphology, characterized by randomized spatial distribution of cells, Fig. 2(c) (see Supplemental Material, SI-V, for simulation movie). The cells organize into a large number of clusters of varying sizes scattered throughout the entire spatial domain occupied by the cells. Individual cells within each cluster appear to move in a less coordinated manner as compared to the case of low noise strength, Fig. 2(d). To better visualize the differences in the cell spatial distribution and the cluster sizes at varying  $\eta$ , we represented the cell positional information using a density plot. The entire spatial domain, in both  $x$  and  $y$  directions, is divided into  $50 \times 50$  bins of equal area. The total number of cells within each bin is color coded, with dark blue representing a low number of cells and dark red representing the highest number of cells. To generate the cell number density heat map, we combined 3 separate simulation results for each value of the noise strength,  $\eta = 0.01, 0.05, 0.2$ , Figs. 2(e)–2(g). The density plots clearly show the strong influence of the noise strength on the cell spatial distribution. For low noise strength,  $\eta = 0.01$ , the cell collective is spatially organized into a thin circular ringlike structure, with patches of high cell density visible at the border. The interior of the domain is characterized by low cell number density, Fig. 2(e). Cells organize themselves into coherently moving clusters with some of the larger clusters containing about 40–50 cells as seen in Fig. 2(e). At higher noise strengths of  $\eta = 0.05$  and 0.2, high cell density patches shift from being confined to the border of the ringlike pattern to its interior. The number of cells within the high cell density patches decreases in a noise strength dependent manner. While 40–50 cells make up the high-density patches for  $\eta = 0.01$ ,  $\sim 30$  cells are visible for  $\eta = 0.2$ . The cell spatial distribution we observe is not a transient feature of the model. Similar behaviors for higher cell division time  $\tau = 2000$  s and longer simulation time (up to  $t = 25\,000$  s), for  $\eta = 0.01$  and  $\eta = 0.2$  confirm that the trend in cell spatial distribution is preserved at longer times (see Supplemental Material, SI-VI). We therefore conclude that the noise-dependent pattern of cell collective behavior is a robust feature of expanding cell collectives.

The velocity vector alignment of individual cells within a cluster, seen in Figs. 2(b) and 2(d), is indicative of collective behavior seen in nonproliferating self-propelled particles [27]. To quantify the collective motion of cells, we measured the order in the motion of the entire cell collective [Fig. 2(h)]. The order parameter is calculated on the basis of position-dependent polarization of the cell velocity by defining a vector pointing from the center of mass of the cell collective to the individual cell position  $\mathbf{c}_i = \mathbf{r}_i - \mathbf{R}_{\text{CM}}$ , where  $\mathbf{R}_{\text{CM}}(t) = (1/N) \sum_i \mathbf{r}_i$  is the center of mass of the whole collective.  $\mathbf{c}_i$  is directed from the center of mass of the cell collective to the cell's position. The angle  $\phi_i$  between a cell's velocity vector,  $\mathbf{v}_i$ , and  $\mathbf{c}_i$  can be calculated from  $\cos(\phi)_i = \mathbf{c}_i \cdot \mathbf{v}_i / (|\mathbf{c}_i| |\mathbf{v}_i|)$

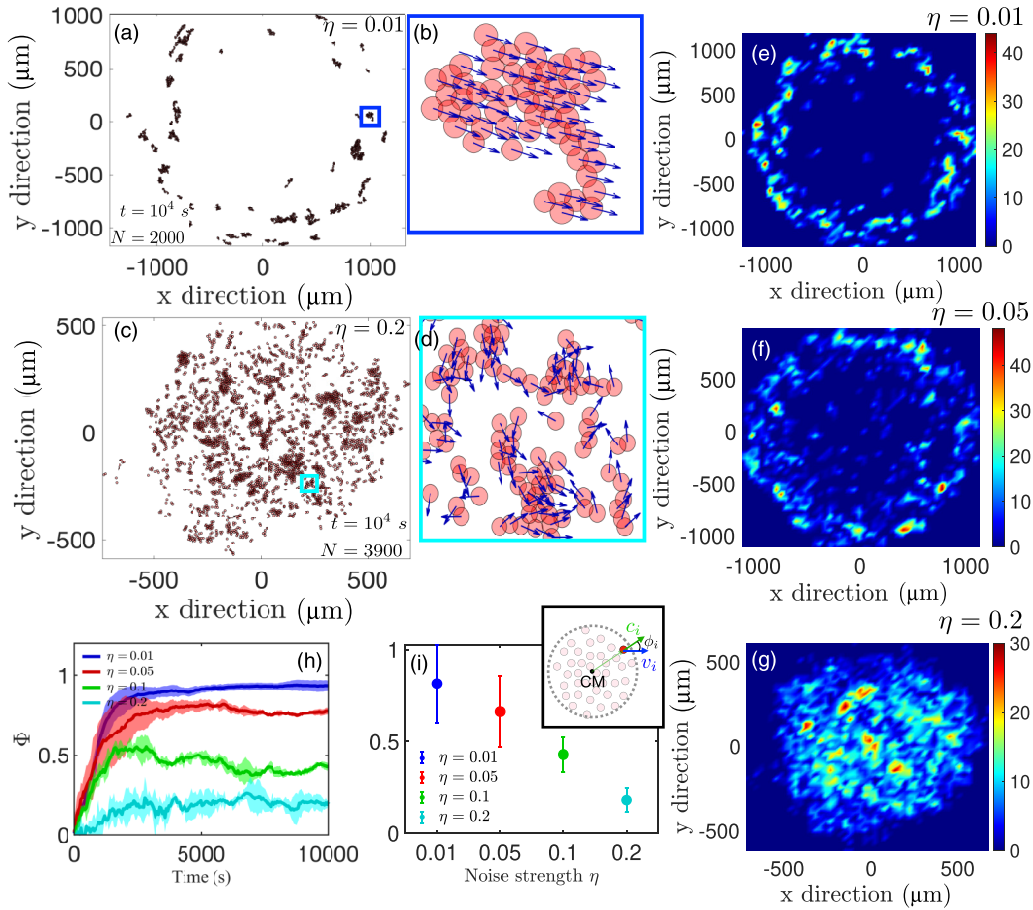


FIG. 2. Noise determines the spatial distribution patterns and collective motion of growing cell collectives. (a)–(b) Spatial distribution of cells at  $t = 10^4$  s for low angular noise ( $\eta = 0.01$ ). Starting from 200 cells, the cell collective grows to  $\sim 2000$  cells distributed among multiple smaller clusters. Cells self-organize into a ringlike pattern, expanding over time as cells proliferate and migrate. The interior of this domain is mostly devoid of cells. Within each cluster, cell movement is highly aligned [see the blue box with a magnified view in panel (b)]. (c)–(d) Spatial distribution of cells at high angular noise  $\eta = 0.2$ , at  $t = 10^4$  s showing  $\sim 3900$  cells. Cell clusters are dispersed all over the spatial domain with the velocity vectors of individual cells appearing more or less to be randomly oriented [see the cyan box and (d) showing a magnified view of a selected spatial region]. (e)–(g) Density plot of the spatial distribution of cells in the collective for (e)  $\eta = 0.01$ , (f)  $\eta = 0.05$ , and (g)  $\eta = 0.2$ , averaging over 3 simulation runs. Color map shows the number of cells in each 2D spatial bin. The difference in the cell spatial distribution pattern is clearly visible, as the noise strength is increased from (e)  $\eta = 0.01$  to (g)  $\eta = 0.2$ . (h) The degree of collective cell motion is quantified using the order parameter  $\Phi$  obtained [see inset of (i)] from the cell velocity vector and cell position vector relative to the center of mass of the cell collective (see main text for the mathematical definition of the order parameter).  $\Phi = 0$  indicates highly disordered motion, in which cells form groups moving in random directions. The temporal behavior of  $\Phi$  shows an initial increase over time and gradually saturates at later times. For  $\eta = 0.2$ ,  $\Phi$  saturates at a value closer to 0, whereas for  $\eta = 0.01$ ,  $\Phi \sim 1$ . The thicker line denotes the mean value and the shaded area is the standard deviation here and henceforth. (i)  $\Phi$  at the final time point decreases as a function of the noise strength  $\eta$ . Inset visualizes the collective order parameter obtained from the relative outward orientation of cell motion  $\phi_i$ . Error bars show the standard deviation here and henceforth.

[see Fig. 2(i) inset]. The orientation order parameter for the whole cell collective is thus defined as

$$\Phi(t) = \frac{1}{N(t)} \sum_i \cos[\phi_i(t)], \quad (12)$$

where  $N$  is the total number of cells.  $\Phi$  can vary between 1 and 0 with  $\Phi = 1$  implying that the  $\mathbf{v}_i$  of every cell is aligned with the position vector  $\mathbf{c}_i$ . The time-dependent behavior of  $\Phi(t)$  shows an initial almost linear increase over time which then saturates at a constant value at later times, Fig. 2(h). For very low noise strength of  $\eta = 0.01$ , the order parameter saturates at  $\sim 1$ , indicating a highly ordered outward cell motion. This is consistent with our observation of highly

coherent and ordered cell movement such that cell velocity orientation  $\mathbf{s}_i$  is aligned with the vector pointing outward toward the periphery of the cell collective,  $\mathbf{c}_i$ . With increasing noise strength,  $\Phi$  progressively gets lower indicating increasingly disordered velocity directions. The orientational order parameter at the final time point decreases with higher noise strengths, Fig. 2(i). This dependence of the order parameter on the noise strength delineates why we obtain markedly distinct spatial distributions of cell collectives. While cells move consistently outward at low noise strengths leading to the emergence of a ringlike pattern, higher noise strengths result in randomized cell movement orientations that lead to a more scattered spatial distribution of cells. In general, our results

map out the emergent spatial distribution of proliferating cell collectives that arises due to noisy cell migration.

#### IV. NOISE IN THE CELL MOTILITY DIRECTION DETERMINES PROLIFERATION AND THE SPREAD OF CELL COLLECTIVE

Having observed angular-noise-dependent differences in the spatial distribution and the orientational order of cell collectives, we next ventured to ask how the noise influences cell division and the growth of the cell collective. As spatial constraints can regulate cell cycle progression during tissue expansion [8,9,32], we anticipate that noise-induced differences in the cell spatial distribution will have an impact on the ability of cells to divide. Particularly, given that we incorporate mechanical feedback on cell division through the force term, noise-induced differences in local cell spatial arrangements could determine the ability of cells to divide. Hence, we quantified the temporal behavior of the total cell number and total spread area of the cell collective, for four different values of the noise strengths  $\eta = 0.01, 0.05, 0.1, 0.2$ . The spatial spread of the migrating cell collective is measured using the radius of gyration squared,

$$R_g^2(t) = \left\langle \frac{1}{N} \sum_{i=1}^N [\mathbf{r}_i(t) - \mathbf{R}_{CM}(t)]^2 \right\rangle. \quad (13)$$

The bracket (...) denotes the ensemble average over 3 different simulation runs. The average squared distance of all the cells from the center of mass is an indicator of the spatial spread or invasion of a cell collective. Small  $R_g^2$  values indicate limited spatial spread of cells, with cells localized close to the center of mass. In contrast, higher values of  $R_g^2$  denote a wider spatial spread due to cells that are located farther away from the center of mass. For a given value of noise strength  $\eta$ , both the total number of cells ( $N$ ) and  $R_g^2$  steadily increase with time, Figs. 3(a) and 3(b). Fitting an exponential function of the form  $ae^{bt}$  to  $N(t)$  allows us to characterize the typical cell division time  $t_D$  based on the fitting parameter  $b$ . Figure 3(c) shows the typical cell number doubling time, defined as  $\ln(2)/t_D$ , and its dependence on noise strength  $\eta$ . At higher noise strengths, the time it takes for the cell number to double is markedly shorter as compared to lower noise strength. To check if these results are dependent on the cell cycle time  $\tau$ , we ran simulations for a longer cell cycle time of  $\tau = 2000$  s as well as a longer total simulation time (25 000 s); see the Supplemental Material [37], SI-VI. The cell spatial distribution in the case of longer cell cycle time ( $\tau = 2000$  s), for both  $\eta = 0.01$  and  $\eta = 0.2$ , is similar to the one we observed in the case of  $\tau = 1000$  s; see the Supplemental Material, Figs. S5A, S5B. Moreover, the cell number and the doubling time showed a similar dependence on the noise strength as was observed in the case of a shorter cell cycle time; see Figs. S5C and S5D in SI-VI of the Supplemental Material. In this case the cell number doubling time was  $\sim 1.7$  h for  $\eta = 0.01$  and  $\sim 1.5$  h for  $\eta = 0.2$  (Fig. S5D). In Figs. 3(d) and 3(e), we show the  $N$  and  $R_g^2$  at the final time point. Surprisingly, at late time points  $N$  and  $R_g^2$  show opposite trends as a function of  $\eta$  [Figs. 3(d) and 3(e)]. The total cell number increases as the noise strength increases [see Fig. 3(d)], implying that stronger fluctuations in the direction of cell movement promote cell proliferation.

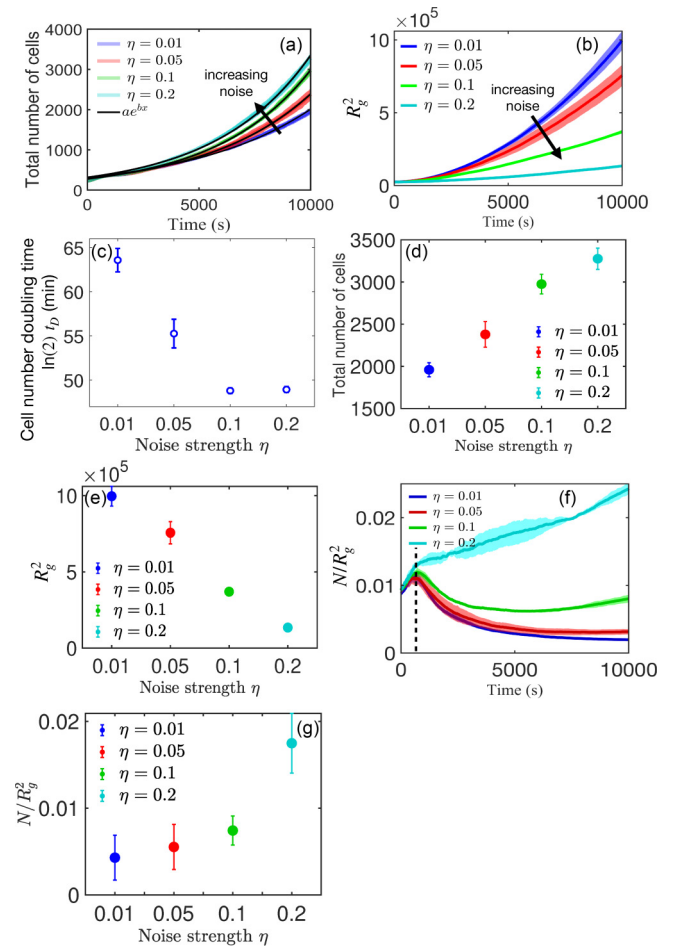


FIG. 3. Noise determines cell proliferation, spatial spread, and packing of growing cell collectives. (a) Temporal behavior of the total number of cells. The time-dependent behavior of cell number shows a pronounced growth at higher noise strengths. An exponential function of time given by  $ae^{bt}$  is fitted to the total number of cells. Fit parameter  $b$  describes the rate at which the cell collective grows and corresponds to typical time  $t_D$  for cell division. (b) Temporal behavior of the total spatial spread of cell collective quantified using the radius of gyration squared  $R_g^2$  ( $\mu\text{m}^2$ ). The cell spatial distribution shows a higher spread at lower noise strengths. (c) Cell number doubling time, given by  $\ln(2)t_D$ , is the typical time it takes for the number of cells to double due to cell division. Cell number doubling time decreases with increasing noise strength. (d) Total number of cells at the final time point  $t = 10\,000$  s as function of the noise strength  $\eta$ . The growth of the cell collective is enhanced at higher noise strengths. Error bars in this and the following figures show the standard deviation. (e) Total spread of cell collective at the final time point  $t = 10\,000$  s as function of the noise strength  $\eta$ . The spatial spread of the cell collective is inversely proportional to the noise strength. (f) We quantify the dynamics of cell spatial packing by evaluating the temporal behavior of the cell number density. At the outset, initially, the cell number density shows a sharp rise over a short duration of time. Thereafter, the cell number density decays over time for noise strengths of  $\eta = 0.01, 0.05$ , and  $0.1$ . For  $\eta = 0.2$ , the cell number density increases at late times. This increase is highly pronounced for  $\eta = 0.2$  and continuously increases over time. (g) Cell number density at  $t = 10\,000$  s as a function of the noise strength  $\eta$ . On average, this indicates that cells are more tightly packed spatially with increasing noise strength.

At  $t = 10\,000$  s, there are  $\sim 3400$  cells for  $\eta = 0.2$ , while  $N \sim 1900$  at  $\eta = 0.01$  is significantly lower compared to the case of  $\eta = 0.2$ , Fig. 3(d). In contrast, the spatial spread of the cell collective showed an inverse dependence on the noise strength  $\eta$ . The spatial spread of the cell collective increases faster over time at lower noise strengths.  $R_g^2$  is an order of magnitude smaller at  $\eta = 0.2$  as compared to  $\eta = 0.01$ , suggesting that as the noise strength increases the cell collective exhibits a more compact spatial distribution [see Fig. 3(e)].

The global quantities  $N$  and  $R_g^2$  describe the time-dependent behavior of the whole cell collective and how it is influenced by noise in the cell motion direction. Taken together with the analysis presented in the preceding section, our results show that increasing the noise strength disrupts cell-cell velocity alignment, as reflected in the lower order parameter, but at the same time promotes cell proliferation, as seen in the higher number of cells and lower cell doubling time. On the other hand, lower noise strength facilitates cell-cell velocity alignment and suppresses cell proliferation.

As collective behavior depends strongly on the number density of actively migrating agents [27], we next sought to understand how cell number density is affected by noise in the direction of cell motility. Given that  $N$  is not fixed and that we impose an open boundary condition, number density is neither fixed nor clearly defined. Nevertheless, we can estimate the cell number density or the overall spatial packing of the cells using  $\rho(t) = N(t)/R_g(t)^2$ , where  $\rho$  is the cell density. Due to the combined effect of cell proliferation and cell motility, both the total number of cells  $N(t)$  and the spatial spread  $R_g^2$ , evolve over time. Consequently,  $\rho(t)$  exhibits a highly dynamic time-dependent behavior initially increasing sharply for each value of noise strength,  $\eta = 0.01, 0.05, 0.1$ , and  $0.2$ , as shown in the time regime before the dashed line in Fig. 3(f). Following the initial rise, its temporal profile for noise strengths  $\eta = 0.01, 0.05, 0.1$  is markedly different from that for  $\eta = 0.2$ . For  $\eta = 0.01, 0.05, 0.1$ , the cell number density decreases over time after the initial transient increase, whereas for  $\eta = 0.2$ , the cell density continues to increase with time, although at a lower rate. At longer times, cell number density is comparatively low for weaker noise strengths.

The cell number density at the final time point rapidly increases with the noise strength, Fig. 3(g). This dependence is rather surprising given our earlier results for the total number of cells as a function of noise strength. We expect higher proliferation to correspond to lower density, due to the role of cell contact force-dependent feedback on proliferation [ $p_i(t)$ ] in our model. When cells are tightly packed in space, we expect the compressing forces on cells from their neighbors to be higher [9,17]. This would restrict cell area growth, eventually leading to lower cell division events due to the force-dependent mechanical feedback term  $p_c$ . Contrary to our expectations, high noise strength leads to a higher cell density and the cell collective has yet a higher number of cells [see Figs. 3(a) and 3(d)]. To investigate this further, we turn to a more detailed quantification of the cell spatial arrangement based on clustering analysis which allows us to quantify how localized changes in cell spatial packing contribute to mechanical feedback on proliferation.

## V. NOISE INCREASES THE NUMBER OF ISOLATED CELLS AND FACILITATES ENHANCED PROLIFERATION

To understand this rather counterintuitive result of higher cell proliferation at higher cell number density, we used a spatial clustering algorithm DBSCAN (density-based spatial clustering of applications with noise) [47] to map out the structure of cell clusters within the collective. The cluster analysis will allow us to ascertain how feedback due to contact force from overlapping cells inhibits cell growth and restrict cell division. Single cells and cells with very few overlapping neighbors will be characterized by the highest proliferative capability due to minimal mechanical feedback on division. On the other hand, we expect fewer cell division events when cells are part of a cluster with a larger number of overlapping cells. Therefore, we anticipate that the size of the cell clusters (i.e., the number of cells in a cluster) might hold the key to understanding why cells in a collective with higher global cell number density proliferate at a higher rate.

DBSCAN is a powerful tool for class identification of clusters in large spatial databases with noise. For cluster identification and classification, DBSCAN requires two input parameters, namely, the maximum cell-cell distance  $\epsilon$  [ $\mu\text{m}$ ] to be considered as a cell's neighbor, and the minimum number of neighboring cells,  $n_{\min}$ , that qualify as a cluster. The DBSCAN algorithm initially labels each cell which has at least  $n_{\min}$  number of cells within a distance of  $\epsilon$  [ $\mu\text{m}$ ] from its center as a core cell. Any cell that has fewer than  $n_{\min}$  number of cells within a distance of  $\epsilon$  [ $\mu\text{m}$ ] from its center is labeled as a border cell. All those cells which have no other cell in their neighborhood within a distance of  $\epsilon$  [ $\mu\text{m}$ ] from their center are labeled as single cells. The algorithm then randomly picks a core cell and assigns it a cluster index. The cluster is expanded sequentially, by adding cells which are in the neighborhood and within the distance of  $\epsilon$  [ $\mu\text{m}$ ] of the randomly picked core cell. In an iterative manner, the DBSCAN algorithm labels each cell as being part of one of the clusters, with each cluster assigned a unique cluster index.

Since only overlapping cells exert growth-inhibiting force on each other, we focused on identifying cell clusters of overlapping cells. Given that the typical cell radii is  $5\ \mu\text{m}$ , we chose  $\epsilon = 9\ \mu\text{m}$ , implying that the cell center-to-center distance between any two cells within a cluster is  $9\ \mu\text{m}$  or less. This value of  $\epsilon$  ensures that only overlapping cells form a cluster. In order to cover the full range of cluster sizes we set  $n_{\min} = 2$ . Using MATLAB's in-built function for DBSCAN [48], with the aforementioned values for the two input parameters ( $\epsilon$  and  $n_{\min}$ ), we identified cell clusters from spatial coordinates of individual cells at the final simulation time point for different  $\eta$  values, Figs. 4(a) and 4(b). Each individual cell cluster in Figs. 4(a) and 4(b) is represented in a different color. DBSCAN is a robust clustering method, allowing for the quantification of additional features of individual cell clusters. Based on the cluster identity of each cell, we can quantify the center of mass and the radius of gyration of individual cell clusters, as shown using circles of different radii in Fig. 4(c).

Our analysis shows that the entire cell collective is spatially organized into cell clusters of different sizes; i.e., cell clusters are composed of varying cell numbers. To ascertain how  $N$

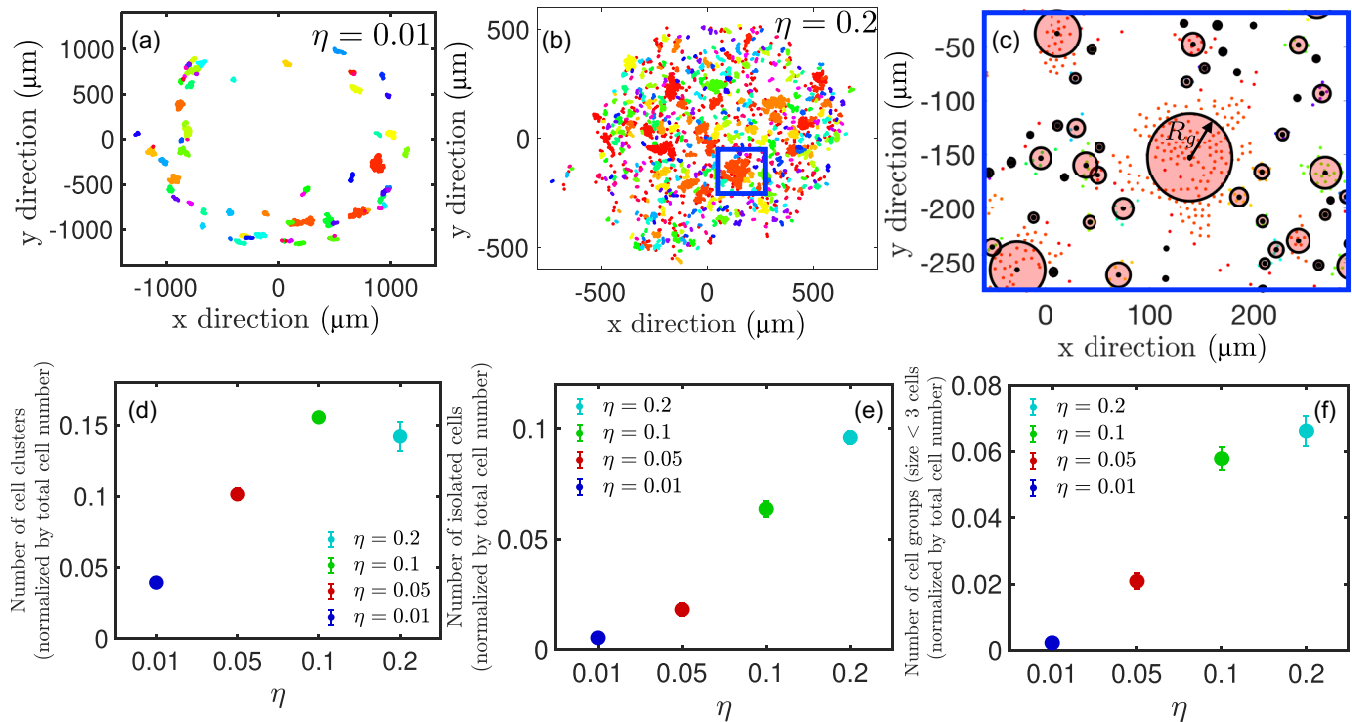


FIG. 4. Noise determines cluster partitioning of growing cell collectives. Clustering analysis of cells using density-based spatial clustering of applications with noise (DBSCAN) organizes the whole cell population into distinct groups. Cells are either assigned to a cluster or labeled as an isolated cell. The dots are not the actual size of the cells. They have been plotted with a radius that corresponds to the maximum cell size of  $5 \mu\text{m}$ . As such the clusters appear to overlap, while they do not overlap in physical space. (a) Cell clusters identified by DBSCAN for low noise strength  $\eta = 0.01$ . Each cluster is given a unique color. (b) Cell clusters identified by DBSCAN for high noise strength  $\eta = 0.2$  with each cluster assigned a unique color. (c) Magnified view of cell clusters with superimposed circles whose radii reflect cluster sizes. Cluster radius is quantified from the radius of the gyration, which is calculated by using the coordinates of the cluster center and the position of each cell in the cluster. (d) Total number of cell clusters increases with noise strength  $\eta$  (at the final simulation time point). (e)–(f) Both (e) the number of single/isolated cells, i.e., cells that are not part of any cluster, as well as (f) the number of clusters with fewer than 3 cells increase with the noise strength  $\eta$ .

varies with the noise strength, we quantified the number of cell clusters at different values of noise strength (normalized by the total number of cells at the final time point). More spatial clusters are formed with increasing noise strength  $\eta$ , Fig. 4(d). The slight dip in the cell cluster number at the highest noise strength of  $\eta = 0.2$  is due to a lower total number of clusters as compared to  $\eta = 0.1$ , which indicates that clusters tend to disintegrate into isolated or single cells when the value of  $\eta$  is increased from 0.1 to 0.2. To understand higher proliferation in cell collectives with higher cell number density we turned our attention to isolated cells and cell clusters with less than 3 cells. We found that both the number of isolated cells and clusters with fewer than 3 cells increases with the noise strength  $\eta$ , Figs. 4(e) and 4(f). These results are robust with respect to cell division and the total simulation time; see the Supplemental Material [37], SI-VI, for runs with longer cell division time ( $\tau = 2000$  s) and simulation time  $t = 25000$  s (results from cluster analysis at longer simulation time are shown in SI-VII of the Supplemental Material). More isolated cells imply that cells can easily grow and divide, without the inhibitory effect of mechanical feedback on cell growth due to cell contact-dependent forces. This scenario is more conducive to cell division, allowing the cell collective to freely grow and divide.

Our DBSCAN-based cell cluster analysis reveals that at higher noise strengths there are large numbers of isolated cells and smaller clusters, leading to enhanced cell proliferation. In an expanding cell collective, cells form clusters as a result of either cell-cell adhesion and/or nearest-neighbor velocity alignment. As the noise strength increases, the tendency for these clusters to disintegrate or breakup increases, due to rapid fluctuations in the direction of migration. The isolated or smaller size clusters then proliferate at a higher rate, thereby increasing the total cell number. Hence, locally, due to the presence of more cells with fewer neighbors, cells can grow and divide relatively unhindered by mechanical feedback. This accounts for the puzzling result where higher noise strengths with higher number density is characterized by enhanced cell proliferation.

## VI. DISCUSSION

The migratory pattern of motile cells is diverse and depends on factors such as whether there is a collection of isolated single cells moving in a uniform direction or a collection of adhesive cells that are physically in contact with each other [12,49,50]. Here, we present an off-lattice agent-based computational modeling framework for expanding 2D

cell collectives with active motility. By focusing on the influence of noise in the direction of a cell's motion, we show that noise strength influences (i) the spatial spread or invasion, and (ii) local cell density-dependent proliferation of cell collectives.

Since the seminal work of Vicsek and co-workers, which has been in many ways foundational to computational modeling-based studies of cell migration [13], there has been growing interest in studying the behavior of collectively migrating cells that undergo proliferation [35,51–54]. The ability to grow and divide is a fundamental property of many biological systems. Our model considers individual cells as active agents that can grow and divide, and whose movement is influenced by their interactions with other cells and stochastic switching in the direction of migration. We take into account various biologically relevant intercellular interactions, such as cell elastic repulsion and cell adhesion [9,17–19], of the type prevalent in confluent tissues [24,55]. The model also includes an additional nearest-neighbor interaction through which cells tend to align the direction of their motion with the average direction of motion of all their neighbors [27]. Given the recent experimental verification that cell proliferation is pressure dependent [31–33], mechanical feedback on proliferation is an important component of our model as the cell area growth depends on the net force acting on the cell from its neighbors. Hence, our model is an important extension of the classical Vicsek model, with self-propelled particles that can undergo growth, birth, and death.

We find that noise strength strongly influences the migratory pattern of cells in the collective. At low noise strengths ( $\eta = 0.01$ ), the cells are sparsely distributed in a ringlike pattern forming clusters of different sizes. Cells in each of these clusters move in a highly ordered manner, with the orientation of cell velocity aligned in the direction away from the center of the cell collective. We quantified this behavior of cell migration using an order parameter whose value is close to 1 for  $\eta = 0.01$ , indicating a highly ordered cell movement. Cell division events in our model scramble the local order of the cell collective as velocity vectors of the daughter cells are assigned random orientations upon division. However, even with these scrambling events present, we notice that the cell collective displays a highly ordered motion at low noise strengths. At intermediate noise strengths ( $\eta = 0.05$ – $0.1$ ), the spatial distribution of migrating cells still shows a ringlike pattern. Although higher density of cells is still confined to the outer ring, clusters and individual cells are to be found in the interior of this domain as well. The orientation order parameter saturates to values much lower than 1 at long times, indicating the onset of a disordered migratory phase. The lower value of the order parameter is due to the formation of smaller cell clusters that move in random directions. As the noise strength is further increased to the highest value considered in this study ( $\eta = 0.2$ ), we observe a clear change in the migratory pattern and spatial arrangement of cells. The cell collective as a whole is split into multiple smaller clusters, with each cluster moving in random directions. The order parameter for the cell collective for such high noise strengths approaches 0, indicating an almost total loss of orientational order in cell motion. Our results show that the noise strength influences the overall spatial distribution and the spread of

the cell collective. The largest spatial spread, compared to the size of the initial distribution of the collective, occurs for very low noise strengths at  $\eta = 0.01$ . In this scenario, cells migrate as a propagating front leading to the emergence of a ringlike pattern. As the noise strength is increased, the spatial spread of the collective is strongly restricted.

An unexpected result of our study is that noise strength influences cell proliferation. Although the total number of cells increases over time for all values of noise strength, the trend in proliferation is strongly dependent on the noise strength. The total number of cells is almost double the number of cells at the final time point for high noise strength  $\eta = 0.2$ , as compared to  $\eta = 0.01$ . Together with our results showing the effect of noise strength on the spatial spread of the cell collective, we find that cell number density is a highly dynamic quantity that increases with noise strength. Taken together, we show that as the noise strength increases, the density of the cell collective increases, whereas the orientational order decreases.

Given the mechanical feedback that limits proliferation due to cell-cell overlap, the increase in cell number with a higher density is a surprising and counterintuitive result. While the overall density indicates that cells should be more tightly packed at higher noise strengths, our DBSCAN-based cluster analysis shows that the local spatial structure is contrary to what is expected. At higher noise strengths, not only are cells distributed into more clusters, but there is also a larger number of isolated cells. Isolated cells are characterized by limited mechanical feedback on division from neighboring cells and can easily proliferate. At lower noise strengths cell clusters contain a larger number of overlapping cells which thus inhibits cell growth and division. In this scenario, cells are localized to the periphery of a ringlike domain while its interior is mostly devoid of cells, leading to the overall density being lower. Therefore, even though cell number density is greater at higher noise strengths, there is a larger number of proliferating cells due to the presence of smaller clusters and more individual cells that are not part of a cluster.

In conclusion, our study demonstrates that angular fluctuations in cell motility direction can strongly determine the spatial distribution of growing cell collectives. Our computational model provides a framework for studying the migration of cells in 2D growing cell collectives. Our model combines cell velocity realignment, as introduced in the Vicsek model, with active growth and cell division. This makes our work highly relevant to study the migration of biological cell collectives together with cell proliferation. Our results imply that there are more, yet unexplained, dynamic behaviors that may emerge from investigating mechanical feedback on proliferation in a system of self-propelled particles undergoing collective motion.

Simulations are carried out using custom code written in MATLAB (R2022a). The codes and the generated data can be found in the GitHub repository [56].

## ACKNOWLEDGMENTS

A.M.-K. acknowledges funding from startup grants. The authors acknowledge the support of Augusta University High Performance Computing Services (AUHPCS) for providing

computational resources contributing to the results presented in this publication. J.E.D acknowledges the support of startup

grants and computing services provided by Whitworth University.

- 
- [1] J. Wu, Z. Mao, H. Tan, L. Han, T. Ren, and C. Gao, Gradient biomaterials and their influences on cell migration, *Interface Focus* **2**, 337 (2012).
- [2] D. Yang, Z. Zhao, F. Bai, S. Wang, A. P. Tomsia, and H. Bai, Promoting cell migration in tissue engineering scaffolds with graded channels, *Adv. Healthcare Mater.* **6**, 1700472 (2017).
- [3] G. Shim, D. Devenport, and D. J. Cohen, Overriding native cell coordination enhances external programming of collective cell migration, *Proc. Natl. Acad. Sci. USA* **118**, e2101352118 (2021).
- [4] C. Giesen, H. A. Wang, D. Schapiro, N. Zivanovic, A. Jacobs, B. Hattendorf, P. J. Schüffler, D. Grolimund, J. M. Buhmann, S. Brandt *et al.*, Highly multiplexed imaging of tumor tissues with subcellular resolution by mass cytometry, *Nat. Methods* **11**, 417 (2014).
- [5] J.-R. Lin, B. Izar, S. Wang, C. Yapp, S. Mei, P. M. Shah, S. Santagata, and P. K. Sorger, Highly multiplexed immunofluorescence imaging of human tissues and tumors using t-CyCIF and conventional optical microscopes, *eLife* **7**, e31657 (2018).
- [6] G. Gaglia, S. Kabraji, D. Rammos, Y. Dai, A. Verma, S. Wang, C. E. Mills, M. Chung, J. S. Bergholz, S. Coy *et al.*, Temporal and spatial topography of cell proliferation in cancer, *Nat. Cell Biol.* **24**, 316 (2022).
- [7] B. I. Shraiman, Mechanical feedback as a possible regulator of tissue growth, *Proc. Natl. Acad. Sci. USA* **102**, 3318 (2005).
- [8] S. J. Streichan, C. R. Hoerner, T. Schneidt, D. Holzer, and L. Hufnagel, Spatial constraints control cell proliferation in tissues, *Proc. Natl. Acad. Sci. USA* **111**, 5586 (2014).
- [9] A. N. Malmi-Kakkada, S. Sinha, X. Li, and D. Thirumalai, Adhesion strength between cells regulates nonmonotonic growth by a biomechanical feedback mechanism, *Biophys. J.* **121**, 3719 (2022).
- [10] B. Ladoux and R. M. Mège, Mechanobiology of collective cell behaviours, *Nat. Rev. Mol. Cell Biol.* **18**, 743 (2017).
- [11] T. E. Angelini, E. Hannezo, X. Trepat, J. J. Fredberg, and D. A. Weitz, Cell migration driven by cooperative substrate deformation patterns, *Phys. Rev. Lett.* **104**, 168104 (2010).
- [12] C. D. Pascalis and S. Etienne-Manneville, Single and collective cell migration: the mechanics of adhesions, *Mol. Biol. Cell* **28**, 1833 (2017).
- [13] E. Méhes and T. Vicsek, Collective motion of cells: from experiments to models, *Integr. Biol.* **6**, 831 (2014).
- [14] S. Kuriyama, E. Theveneau, A. Benedetto, M. Parsons, M. Tanaka, G. Charras, A. Kabla, and R. Mayor, In vivo collective cell migration requires an LPAR2-dependent increase in tissue fluidity, *J. Cell Biol.* **206**, 113 (2014).
- [15] C. Huang, K. Jacobson, and M. D. Schaller, Map kinases and cell migration, *J. Cell Sci.* **117**, 4619 (2004).
- [16] M. Melani, K. J. Simpson, J. S. Brugge, and D. Montell, Regulation of cell adhesion and collective cell migration by hindsight and its human homolog RREB1, *Curr. Biol.* **18**, 532 (2008).
- [17] A. N. Malmi-Kakkada, X. Li, H. S. Samanta, S. Sinha, and D. Thirumalai, Cell growth rate dictates the onset of glass to fluidlike transition and long time superdiffusion in an evolving cell colony, *Phys. Rev. X* **8**, 021025 (2018).
- [18] S. Sinha, A. N. Malmi-Kakkada, X. Li, H. S. Samanta, and D. Thirumalai, Spatially heterogeneous dynamics of cells in a growing tumor spheroid: Comparison between theory and experiments, *Soft Matter* **16**, 5294 (2020).
- [19] S. Sinha and A. N. Malmi-Kakkada, Interparticle adhesion regulates the surface roughness of growing dense three-dimensional active particle aggregates, *J. Phys. Chem. B* **125**, 10445 (2021).
- [20] J. E. Dawson, T. Sellmann, K. Porath, R. Bader, U. van Rienen, R. Appali, and R. Koehling, Cell-cell interactions and fluctuations in the direction of motility promote directed migration of osteoblasts in direct current electrotaxis, *Front. Bioeng. Biotechnol.* **10**, 1 (2022).
- [21] X. Yang, M. L. Manning, and M. C. Marchetti, Aggregation and segregation of confined active particles, *Soft Matter* **10**, 6477 (2014).
- [22] M. L. Woods, C. Carmona-Fontaine, C. P. Barnes, I. D. Couzin, R. Mayor, and K. M. Page, Directional collective cell migration emerges as a property of cell interactions, *PLoS ONE* **9**, e104969 (2014).
- [23] S. Battersby, News feature: The cells that flock together, *Proc. Natl. Acad. Sci. USA* **112**, 7883 (2015).
- [24] G. Grégoire, H. Chaté, and Y. Tu, Moving and staying together without a leader, *Physica D (Amsterdam, Neth.)* **181**, 157 (2003).
- [25] A. Buttenschön and L. Edelstein-Keshet, Bridging from single to collective cell migration: A review of models and links to experiments, *PLoS Comput. Biol.* **16**, e1008411 (2020).
- [26] R. J. Huebner, A. N. Malmi-Kakkada, S. Sarikaya, S. Weng, D. Thirumalai, and J. B. Wallingford, Mechanical heterogeneity along single cell-cell junctions is driven by lateral clustering of cadherins during vertebrate axis elongation, *Elife* **10**, e65390 (2021).
- [27] T. Vicsek, A. Czirók, E. Ben-Jacob, I. Cohen, and O. Shochet, Novel type of phase transition in a system of self-driven particles, *Phys. Rev. Lett.* **75**, 1226 (1995).
- [28] R. N. Binny, M. J. Plank, and A. James, Spatial moment dynamics for collective cell movement incorporating a neighbour-dependent directional bias, *J. R. Soc. Interface.* **12**, 20150228 (2015).
- [29] P. K. Mishra and S. Mishra, Active polar flock with birth and death, *Phys. Fluids* **34**, 057110 (2022).
- [30] M. A. Heinrich, R. Alert, J. M. LaChance, T. J. Zajdel, A. Košmrlj, and D. J. Cohen, Size-dependent patterns of cell proliferation and migration in freely-expanding epithelia, *eLife* **9**, e58945 (2020).
- [31] G. Helmlinger, P. A. Netti, H. C. Lichtenbeld, R. J. Melder, and R. K. Jain, Solid stress inhibits the growth of multicellular tumor spheroids, *Nat. Biotechnol.* **15**, 778 (1997).
- [32] I. Di Meglio, A. Trushko, P. Guillamat, C. Blanch-Mercader, S. Abuhattum, and A. Roux, Pressure and curvature control of the cell cycle in epithelia growing under spherical confinement, *Cell Rep.* **40**, 111227 (2022).

- [33] B. Alric, C. Formosa-Dague, E. Dague, L. J. Holt, and M. Delarue, Macromolecular crowding limits growth under pressure, *Nat. Phys.* **18**, 411 (2022).
- [34] G. Zills, T. Datta, and A. N. Malmi-Kakkada, Enhanced mechanical heterogeneity of cell collectives due to temporal fluctuations in cell elasticity, *Phys. Rev. E* **107**, 014401 (2023).
- [35] D. Drasdo and S. Höhme, A single-cell-based model of tumor growth *in vitro*: Monolayers and spheroids, *Phys. Biol.* **2**, 133 (2005).
- [36] G. Schaller and M. Meyer-Hermann, Multicellular tumor spheroid in an off-lattice Voronoi-Delaunay cell model, *Phys. Rev. E* **71**, 051910 (2005).
- [37] See Supplemental Material at <http://link.aps.org/supplemental/10.1103/PhysRevResearch.6.033054> for additional details of the simulation methods and verifications.
- [38] H. Yoon, T. S. Kim, and T. J. Braciale, The cell cycle time of CD8<sup>+</sup> T cells responding *in vivo* is controlled by the type of antigenic stimulus, *PLoS ONE* **5**, e15423 (2010).
- [39] S. Chen, N. Li, S. F. Hsu, J. Zhang, P. Y. Lai, C. K. Chan, and W. Chen, Intrinsic fluctuations of cell migration under different cellular densities, *Soft Matter* **10**, 3421 (2014).
- [40] D. Caballero, R. Voituriez, and D. Riveline, Protrusion fluctuations direct cell motion, *Biophys. J.* **107**, 34 (2014).
- [41] G. Volpe and G. Volpe, Simulation of a Brownian particle in an optical trap, *Am. J. Phys.* **81**, 224 (2013).
- [42] M. Plodinec, M. Loparic, C. A. Monnier, E. C. Obermann, R. Zanetti-Dallenbach, P. Oertle, J. T. Hyotyla, U. Aebi, M. Bentires-Alj, R. Y. Lim *et al.*, The nanomechanical signature of breast cancer, *Nat. Nanotechnol.* **7**, 757 (2012).
- [43] K. L. Butler, V. Ambravaneswaran, N. Agrawal, M. Bilodeau, M. Toner, R. G. Tompkins, S. Fagan, and D. Irimia, Burn injury reduces neutrophil directional migration speed in microfluidic devices, *PLoS ONE* **5**, e11921 (2010).
- [44] R. Milo, P. Jorgensen, U. Moran, G. Weber, and M. Springer, Bionumbers—the database of key numbers in molecular and cell biology, *Nucleic Acids Res.* **38**, D750 (2010).
- [45] N. I. Petridou, B. Corominas-Murtra, C.-P. Heisenberg, and E. Hannezo, Rigidity percolation uncovers a structural basis for embryonic tissue phase transitions, *Cell* **184**, 1914 (2021).
- [46] N. I. Petridou, S. Grigolon, G. Salbreux, E. Hannezo, and C.-P. Heisenberg, Fluidization-mediated tissue spreading by mitotic cell rounding and non-canonical Wnt signalling, *Nat. Cell Biol.* **21**, 169 (2019).
- [47] M. Ester, H.-P. Kriegel, J. Sander, and X. Xu, A density-based algorithm for discovering clusters in large spatial databases with noise, in *KDD '96: Proceedings of 2nd International Conference on Knowledge Discovery and Data Mining* (ACM, 1996).
- [48] Matlab version 9.11.0.1837725 (R2021b), <https://www.mathworks.com/help/stats/dbscan.html>.
- [49] G. Malet-Engra, W. Yu, A. Oldani, J. Rey-Barroso, N. S. Gov, G. Scita, and L. Dupré, Collective cell motility promotes chemotactic prowess and resistance to chemorepulsion, *Curr. Biol.* **25**, 242 (2015).
- [50] M. Lintz, A. Muñoz, and C. A. Reinhart-King, The mechanics of single cell and collective migration of tumor cells, *J. Biomech. Eng.* **139**, 021005 (2017).
- [51] A. Ghaffarizadeh, R. Heiland, S. H. Friedman, S. M. Mumenthaler, and P. Macklin, PhysiCell: An open source physics-based cell simulator for 3-D multicellular systems, *PLoS Comput. Biol.* **14**, e1005991 (2018).
- [52] J. Zimmermann, B. A. Camley, W. J. Rappel, and H. Levine, Contact inhibition of locomotion determines cell-cell and cell-substrate forces in tissues, *Proc. Natl. Acad. Sci. USA* **113**, 2660 (2016).
- [53] K. Kaiyrbekov, K. Endresen, K. Sullivan, Z. Zheng, Y. Chen, F. Serra, and B. A. Camley, Migration and division in cell monolayers on substrates with topological defects, *Proc. Natl. Acad. Sci. USA* **120**, e2301197120 (2023).
- [54] P. Van Liedekerke, A. Buttenschön, and D. Drasdo, Off-lattice agent-based models for cell and tumor growth: Numerical methods, implementation, and applications, in *Numerical Methods and Advanced Simulation in Biomechanics and Biological Processes* (Elsevier, Amsterdam, The Netherlands, 2018), pp. 245–267.
- [55] F. Peruani, F. Ginelli, M. Bär, and H. Chaté, Polar vs. apolar alignment in systems of polar self-propelled particles, *J. Phys.: Conf. Ser.* **297**, 012014 (2011).
- [56] See [https://github.com/Edjon85/proliferating\\_cells\\_collective\\_motion/tree/main](https://github.com/Edjon85/proliferating_cells_collective_motion/tree/main).